Deep-Sea Research Part II 147 (2018) 43–57

Contents lists available at ScienceDirect

Deep-Sea Research Part II

journal homepage: www.elsevier.com/locate/dsr2

Hydrographic trends in Prince William Sound, Alaska, 1960–2016

Robert W. Campbell

Prince William Sound Science Center, Cordova, AK, USA

A B S T R A C T

A five-decade time series of temperature and salinity profiles within Prince William Sound (PWS) and the immediately adjacent shelf was assembled from several archives and ongoing field programs, and augmented with archived SST observations. Observations matched with recent cool (2007–2013) and warm (2013-onward) periods in the region, and also showed an overall regional warming trend (~ 0.1 to 0.2 °C decade^{-1}) that matched long-term increases in heat transport to the surface ocean. A cooling and freshening trend (~ − 0.2 °C decade^{-1} and 0.02 respectively) occurred in the near surface waters in some portions of PWS, particularly the northwestern margin, which is also the location of most of the ice mass in the region; discharge (estimated from other studies) has increased over time, suggesting that those patterns were due to increased meltwater inputs. Increases in salinity at depth were consistent with enhanced entrainment of deep water by estuarine circulations, and by enhanced deep water renewal caused by reductions in downwelling-favorable winds. As well as local-scale effects, temperature and salinity were positively cross correlated with large scale climate and lunar indexes at long lags (years to months), indicating the longer time scales of atmospheric and transport connections with the Gulf of Alaska. Estimates of mixed layer depths show a shoaling of the seasonal mixed layer over time by several meters, which may have implications for ecosystem productivity in the region.

1. Introduction

Prince William Sound (PWS) is a large and complicated estuarine-fjord system with numerous sub-basins around its margins. It is separated from the Gulf of Alaska (GoA) by several large islands, and surrounded on its three landward sides by the Chugach mountains. The marine ecosystem in the PWS region is extremely productive, and supports several groundfish and salmon fisheries that are of considerable importance to the local economy. The region is also a locally important transport corridor for oil tankers travelling to and from the terminus of the Trans-Alaska Pipeline in Valdez, cruise ships, and cargo vessels.

The surface waters of the continental shelf adjacent to PWS are dominated by the relatively fresh Alaska Coastal Current and the Copper River, which is the largest point source of fresh water to the northern GoA (Stabeno et al., 2004). PWS is connected to the coastal GoA through two main entrances, Hinchinbrook Entrance (HE) and Montague Strait (MS), with surface waters generally entering through HE and exiting through MS, although reflux events do occur. Deepwater renewal events generally occur through HE during summer and autumn (Halverson et al., 2012). The surface waters of PWS also receive freshwater from countless streams, small rivers, and icefields along the periphery, as well as considerable sediment loading (Beamer et al., 2016; Feeley, 1979; Gay and Vaughan, 2001; Hill et al., 2015). Precipitation in the region is prodigious, with order of 95 km^3 of fresh water moving through the system each year, accounting for 11% of all freshwater discharge into the GoA (Neal et al., 2010; Beamer et al., 2016). Recent evidence (Arendt et al., 2013; Barclay et al., 2013; Beamer et al., 2016; Wiles et al., 1999) suggests that losses of ice mass in the GoA region have been considerable, which may have increased discharge into to the coastal ocean. Over the continental shelf, near-surface salinity has been declining over time (Royer and Grosch, 2006).

Warming trends have been observed globally for many years (Levitus et al., 2001), and those trends have also been observed in Alaska (Shulski and Wendler, 2008). Much of the increased heat flux has been taken up by the ocean (Barnett et al., 2005), and warming trends have been observed in coastal Alaska at the regularly sampled GAK line near Seward, AK (Royer and Grosch, 2006; Janout et al., 2010). Since late 2013, sea surface temperature anomalies throughout the GoA have been as much as 3–4 °C above average; the leading hypothesis for that particular anomaly (colloquially referred to as “The Blob”) is a reduction in winter heat flux leading to residual heat being retained by the surface ocean (Bond et al., 2015). 2015–2016 was also the second strongest El Niño event on record (NOAA, 2016), which generally correlates with higher that average surface temperatures.

Although there is a well-maintained time series of the coastal GoA in the GAK line, there has not been a comparable coordinated long-term effort in Prince William Sound. Prior to the 1989 Exxon Valdez Oil Spill,

E-mail address: rcampbell@pwssc.org.

http://dx.doi.org/10.1016/j.dsr2.2017.08.014

Available online 26 August 2017

oceanographic observations were sparse and scattered, with the Outer Continental Shelf Environmental Assessment Program (1974–1981) representing one of the few larger-scale efforts. Following the spill, there were several large field campaigns, including the Sound Ecosystem Assessment (1992–1998), Global Ocean Ecosystem Dynamics (1997–2004) and Gulf Watch Alaska projects (2009-present). However, sampling by those projects was also episodic, and in many cases visited different stations in different parts of PWS at different times. Given the trends observed elsewhere, it can be expected that there have been changes in the PWS region as well. It is therefore the goal of this study to assemble the many hydrographic (temperature and salinity) observations that have been made in the PWS region to produce a time series of observations, and to examine those time series to describe how the hydrography and oceanography of the region has changed, with reference to the oceanic and atmospheric forcing that drive the system.

2. Methods

2.1. Data sources

Profiles of temperature and salinity were collected from several sources. The database described by Musgrave et al. (2013) was used, which includes casts taken between 1973 and 2010 by several coordinated projects and various methods (STD, CTD, XCTD, XBT), which was merged with casts from the NOAA NODC World Ocean Database. Casts in the database were verified with automated methods to eliminate duplicate casts and to check for physically unlikely values ($-2\ ^{\circ}C < T > 25\ ^{\circ}C$, $0 < S > 35$); questionable casts were visually examined prior to being discarded.

Casts taken as part of recent oceanographic monitoring programs conducted by the author were also included. Those data were collected from 2009 to present at 12 standard stations in the PWS region with a Seabird Electronics SBE19 or SBE25 CTD. Casts were processed with the standard Seabird Data Processing routines (available from www.seabird.com) and calibrations were done annually. Salinity is reported on the Practical Salinity Scale (PSS-78). For analysis, the casts were grouped into four areas corresponding to the adjacent Gulf of Alaska Shelf (GoA), central Sound (CS), east (E) and northwest (NW) regions defined by Musgrave et al. (2013; Fig. 1). There were 2126, 3764, 540 and 4568 individual profiles within the GoA, CS, E and NW domains, respectively.

Profile data are often missing surface observations (profiles in the database usually began at 1 or 2 m depth, occasionally deeper), and it is at the surface that significant changes in atmospheric and freshwater forcing are most likely to occur; surface observations are more frequent, and also have a slightly longer time series available. For this study, Sea Surface Temperature (SST) from the International Comprehensive Ocean-Atmosphere Data Set (ICOADS) release 3.0 was used (National Centers for Environmental Information et al., 2016), with enhanced filtering tags set. SST data were sparse in the PWS region prior to 1960, and data prior to January 1st of that year were not used. The SST data were also assigned to the four spatial domains (see Fig. 1) and there were 590,598, 513,234, 1138 and 364,047 individual casts in the GoA, CS, E and NW domains, respectively.

The net turbulent heat flux (the sum of latent and sensible heat fluxes, which are highly correlated) was estimated from the nearest gridpoint of the National Centers for Environmental Prediction (NCEP) reanalysis (Kalnay et al., 1996), NCEP Reanalysis data were provided by the NOAA/OAR/ESRL PSD, Boulder, Colorado, USA (http://www.esrl.noaa.gov/psd/). Radiative heat fluxes were ignored because the turbulent terms dominate and for comparison with prior work (Janout et al., 2010).The grid point (60°N 146°15′W) is approximately 44 km south of Hinchinbrook Entrance, on the adjacent shelf. Heat fluxes from the NCEP reanalysis were compared to heat flux estimates calculated at several National Data Buoy Center (NDBC) buoys in the region (buoys 46,060, 46,061, 46,082, 46,085 and 46,076) using the TOGA-COARE algorithm (Fairall et al., 1996) and were found to be well correlated (r^2 values of 0.60–0.67 with $p < 0.05$). NCEP estimates were used in this study because they encompass the entire temporal range of the other datasets, while the buoy records begin in 1995 or later. Heat flux estimates were converted to seasonally detrended anomalies by subtracting observations from daily averages, and monthly averages calculated from the daily anomalies.

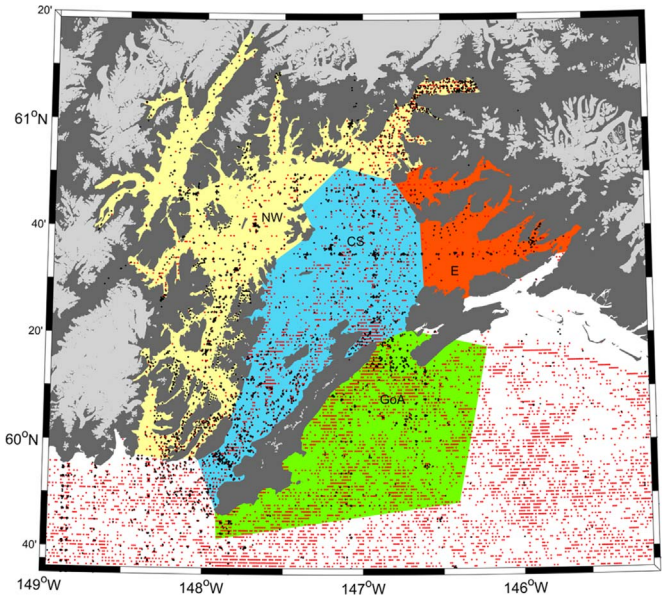

Fig. 1. Position of CTD casts in the CTD database (black dots) and ICOADS SST observations (red dots) used in this study, and geographic regions assigned to the casts. E = eastern (red) Prince William Sound NW = northwest PWS (yellow); CS = central PWS (blue); GoA = Gulf of Alaska (green). Glacier and ice sheet coverage over land from the Randolph Glacier Inventory (version 3.2) is shown in light grey; ice extent data was downloaded from http://www.glims.org/RGI/rgi32_dl.html. (For interpretation of the references to color in this figure legend, the reader is referred to the web version of this article.)

As a proxy for wind-driven transport into PWS (Halverson et al., 2012), the offshore component of the NOAA Pacific Fisheries Environmental Laboratory monthly upwelling index (http://oceanwatch.pfel.noaa.gov/products/PFELData/upwell/monthly/upanoms.mon) at 60°N 146°W was used. The format of the upwelling index was the same as the heat flux estimates, and monthly anomalies were calculated with the same method.

Precipitation records in the PWS are sparse and there are few long-term time series. To estimate precipitation to the region, NOAA CMAP precipitation estimates provided by the NOAA/OAR/ESRL PSD, Boulder, Colorado, USA were used (http://www.esrl.noaa.gov/psd/; Xie and Arkin, 1997). Monthly averages at four grid points bracketing the PWS area (longitudes 148° 45′W and 151° 15′W and latitudes 58° 45′N and 61° 15′N) were averaged, and anomalies calculated by subtracting the long-term mean (from 1981 to 2010, also provided by the NOAA PSD). Freshwater discharge estimates into PWS were taken from Beamer et al. (2016) available at (http://www.aoos.org). Discharge in each coastal cell within PWS (i.e. the CS, E and NW regions) was summed for each model day, converted to a daily anomaly, and averaged monthly.

In order to relate the conditions within PWS to larger scale climatic trends, cross correlations were determined between temperature and salinity and large-scale climate indices. The Pacific Decadal Oscillation (PDO: Mantua et al., 1999) is the first principal component of North Pacific SST and was downloaded from the University of Washington JISAO PDO page (http://research.jisao.washington.edu/pdo/). The North Pacific Gyre Oscillation (NPGO: Di Lorenzo et al., 2008), the second principal component of sea surface height anomaly, is

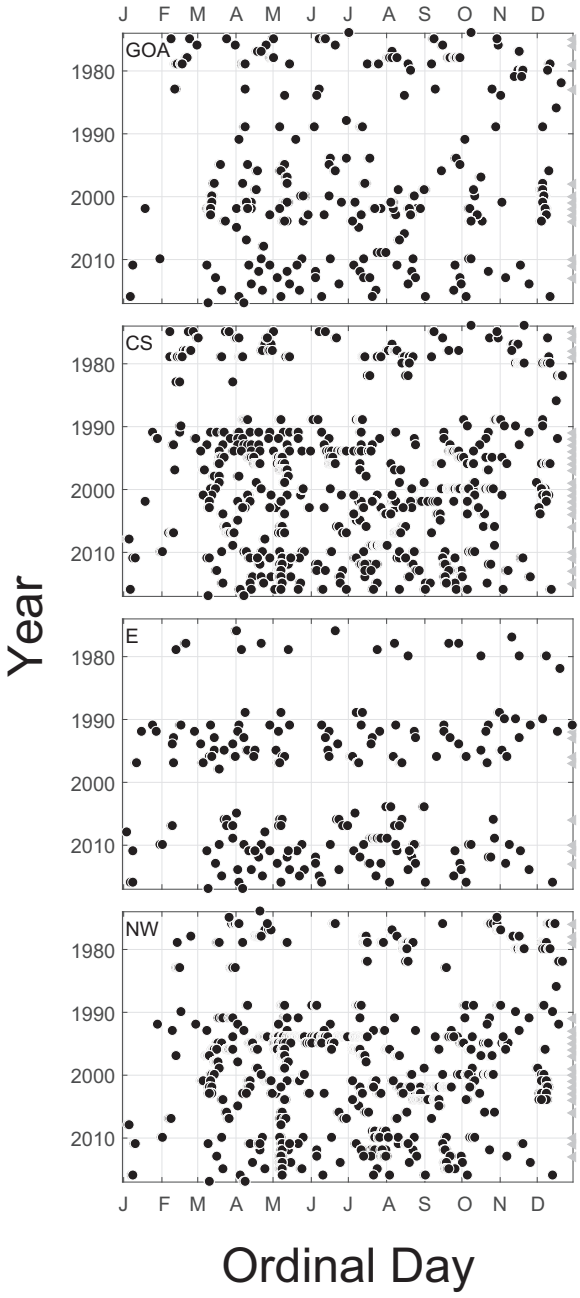

Fig. 2. Inter- and intra-annual coverage of the CTD casts used in this study, broken out into the four Prince William Sound geographic regions (Fig. 1). Each dot denotes a cast. Years that were found to have an adequate number of casts to define the annual cycle (> 6 observations, with an observation in each quarter, see text) are denoted with triangles along the ordinate.

uncorrelated with the PDO, and reflects changes in the intensity of gyre circulations in the North Pacific. Values of the NPGO index were obtained from http://www.o3d.org/npgo/.

2.2. Data analysis

The datasets used in this study presented a number of analysis challenges caused by the spatial and temporal heterogeneity of the samples, as is to be expected when using archived data from numerous different projects with different goals. Assigning the observations into spatial domains attempts to remove the effect of spatial heterogeneity in the dataset by combining stations that can be expected to be similar (a discussion of the choice of the regions is given by Musgrave et al., 2013). The observations in the dataset were also temporally scattered (Fig. 2), which created a challenge for standard time series and frequency domain methods that require a regularly sampled time series. Breaking the observations up into categorical time categories (i.e. weekly, monthly) is undesirable, because the region has large seasonal changes in hydrographic properties (e.g. Xiong and Royer, 1984; Wang et al., 2001; Royer, 2005), and thus the date and time an observation was made has value. It was therefore decided to use a simple regression and harmonic analysis that explicitly includes time to examine trends (Wilks, 2011).

All regressions calculated in this study were by nonlinear least squares using a Trust Region Reflective algorithm (Branch et al., 1999), with a termination tolerance of 10^{-6}. No constraints were set on the number of iterations, but they were always < 600. Initial parameter estimates were set to zero, except for constants ($\bar{y}$ and β_0, see below) which were initialized as the mean of all observations being fit. Confidence intervals were calculated at the 95% level.

If not already binned, casts were averaged into 1-m depth bins starting with the 2-m bin. Depth specific fits to the entire dataset showed that a second order cosine curve of the following form tended to describe the seasonal cycle in temperature and salinity reasonably well:

$$H_z(t) = \bar{y} + \sum_{k=1}^{2} C_k \cos\left[\frac{2\pi k t}{365} - \varphi_k\right] \quad (1)$$

where H is the hydrographic quantity of interest (temperature or salinity, for a specific depth, z), t is the day of the year (i.e. a number between 1 and 365.25) and $\bar{y}$, C_k and φ_k are fitted parameters. The constant, $\bar{y}$, may be thought of as the seasonally detrended average, while C_k and φ_k describe the amplitude and phase respectively of the components. With k = 1 and 2, the model contains an annual and a semiannual component. Prior work in the region (e.g. Royer et al., 2001) have used a first order equation (e.g. k = 1 only), but it was found with the current dataset that a second order model gave a better fit (as diagnosed with an *F*-test), particularly in the upper part of the water column; a third order model was not a significant improvement (*F*-test p = 1.0, at all depths).

Fitting the data by depth bins for the entire dataset (and within each spatial domain) thus produces a climatological annual cycle for that depth that may be put together into a depth-specific climatological annual cycle (Fig. 3). Similarly, seasonal climatologies were produced for MLD, surface heat flux, and the NOAA upwelling index (Fig. 4).

Eq. (1) may also be extended to a simple regression model that may be fit to the entire time series, again for each depth:

$$H_z(d) = \beta_0 + \beta_1 t + \sum_{k=1}^{2} C_k \cos\left[\frac{2\pi k d}{365} - \varphi_k\right] \quad (2)$$

where d is the date number, a fractional number of days from an arbitrary date and time (in this study, the reference date number was set such that date number 1 was January 1, 0000), β_0 is the constant, β_1 the linear trend, and the rest of the parameters are as in Eq. (1). The advantage of this regression method is that it can span gaps in the time series; the disadvantage is that the parameters of the harmonics are fit for the entire dataset, and may in fact change over time (e.g. changes in minimum or maximum temperatures, or the timing of the annual cycle).

To incorporate interannual variability in the timing and the magnitude of the annual cycle, Eq. (1) was also fit to individual years (January 1 through December 31). Because the data are patchy in time, individual years were included in the analysis only if (1) there were > 6 observations made over the course of the year, and (2) the observations were distributed such that there were observations made within each quarter of the year. The choice of quarters was arbitrary, and was intended to ensure that there was a good enough temporal spread of observations over the year to reasonably describe the annual cycle.

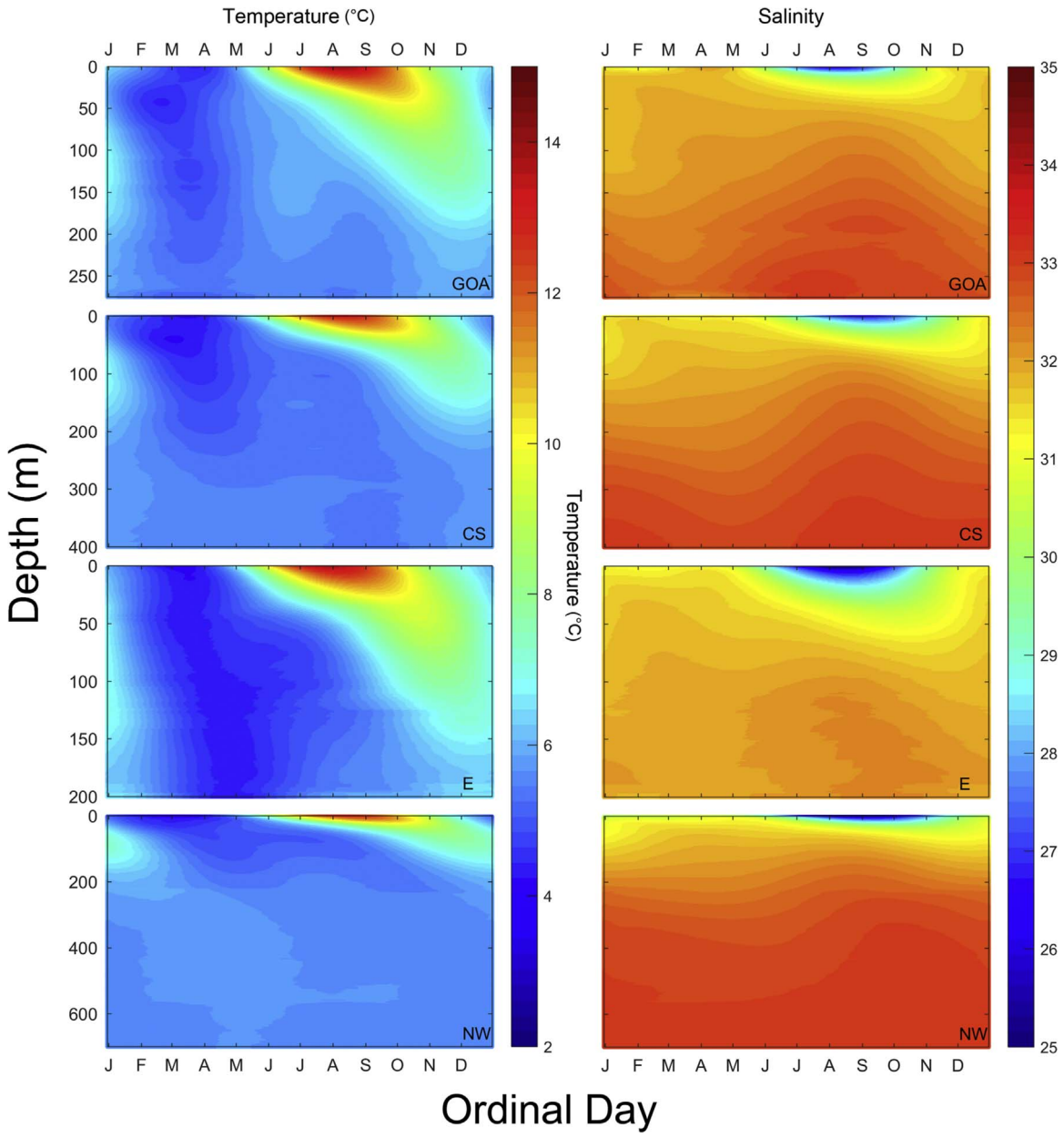

Fig. 3. Climatological annual temperature (°C, left panels) and salinity (right panels) cycles in each of the Prince William Sound geographic regions (Fig. 1). Each annual cycle was created by fitting Eq. (1) to each depth bin in a stepwise fashion, (see text). Note that the scaling of the ordinate changes among regions.

Temporal coverage was best at the surface and tended to decline at depth. After fitting Eq. (1) to each depth bin in each spatial domain, the changes in $\bar{y}$, C_k and φ_k were regressed over time to test for trends. This analysis is referred to as an "annual" analysis, because parameters were calculated for each entire year that met the data density criteria.

Changes in the depth of the surface mixed layer have been observed in time series elsewhere in the GoA (Li et al., 2005; Weingartner, 2007), although not on the nearby coastal shelf (Sarkar et al., 2005); changes in heat or freshwater fluxes might result in changes in PWS. In this study, mixed layer depth (MLD) was estimated with a simple threshold method (Thomson and Fine, 2003; Musgrave et al., 2013) based on the differences in potential density at the surface versus at depth. MLD was defined as the depth (z) where the difference in potential density ($\Delta\rho_\theta = \rho_\theta(z) - \rho_\theta(z_0)$) at depth and the surface (z_0) exceeded 0.125 kg m^{-3}. The threshold was selected to be an estimate of the depth of the seasonal pycnocline (Thomson and Fine, 2003). MLD is much more susceptible to short term-variations by wind mixing, was much more variable than temperature and salinity measurements, and did not have as coherent a seasonal structure. MLD estimates were seasonally detrended and converted to anomalies by subtracting observations from a 10-day moving average of MLD versus ordinal day from the entire dataset, then combined into quarterly averages.

Lag-lead relationships between hydrographic properties (T and S anomalies) and the large-scale climatic indices (PDO, NPGO) and Lunar Nodal Cycle (LNC; see below) were examined with cross correlations (Pearson's). Cross correlations were estimated for each 1-m depth bin within each geographic region. The PDO and NPGO indices are reported monthly, and anomalies (calculated from the entire dataset) were assigned to calendar months for each correlation. LNC lags were computed from the time associated with each observation. The significance of each correlation was assessed with simulated probability distribution functions (10,000 permutations) of correlation coefficients generated from two red noise time series estimated from the anomalies and indexes (Di Lorenzo et al., 2008).

The ICOADS SST observations are complimentary to the cast data, but are of difference provenance (and longer temporal resolution), so

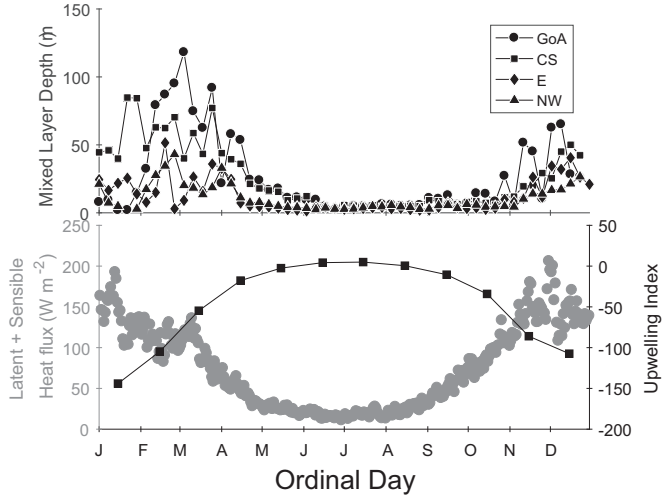

Fig. 4. Annual climatologies of mixed layer depth (MLD; top panel) and surface heat flux (bottom panel, grey symbols, left axis) in Prince William Sound and the nearest NOAA upwelling index (bottom panel, black symbols, right axis). Daily MLD averages were linearly interpolated to weekly values to reduce clutter to better allow comparison among the geographic regions. A positive upwelling index indicates coastal upwelling, a negative index indicates downwelling.

were treated separately in this analysis. SST was converted to anomalies by subtracting observations from the long-term climatology (Eq. (1)) and regressed over time with a linear model (which is equivalent to fitting Eq. (1)).

2.3. Lunar nodal tide

As well as long term trends that can be expected to follow as a result of global and basin scale changes, it has been shown that there is a low frequency component to air and sea surface temperatures set up by the 18.6-year lunar declination cycle (Loder and Garrett, 1978; Royer, 1993; McKinnell and Crawford, 2007). As well as linear fits to the parameters, the progression of the 18.6-year nodal tide was estimated with the cosine of the negative of the longitude of the Moon's ascending node, N′ (Doodson, 1921):

$$N' = 100°0.8432 + 1934°0.1420T - 0°0.0021T^2 \quad (3)$$

where T is time, based on a Julian century of 36,525 solar days, with time zero at 00:00 January 1, 1900; the cosine of N' shall be referred to as the Lunar Nodal Cycle (LNC). The LNC was cross correlated with temperature and salinity to determine the dominant lags.

3. Results

3.1. CTD time series

The slope of the simple regression model (Eq. (2)) applied to the cast data in each 1-m depth bin indicated a significant warming trend in the GoA region at all depths, and a warming trend at depth in central PWS and the NW region (Fig. 5). Near-surface and near-bottom trends in the E region had confidence intervals that spanned zero, and thus were not significant (the E region had the smallest number of casts and the poorest temporal coverage); there was a significant warming trend in the mid-depths. There was a significant cooling trend in the NW region between 3 and 23 m. There was a trend toward increasing salinity at depth in the GoA and CS regions, and at mid-depths (~ 100 to 250 m) in the NW region (Fig. 6). Regression models incorporating an 18.6-year component resulted in fits with confidence intervals for the coefficients that spanned zero and are not shown.

The trends in the parameters from the annual model fits returned similar results with significant trends in the $\bar{y}$ term, also indicating a warming trend at depth in the GoA region, and over most depths in the CS region (Fig. 7, left panel); there were few significant trends in salinity: there was near-surface freshening in the NW region and a trend towards higher salinity at depth in the CS region (and ~ 205 to 225 m in the GoA region). The annual amplitude component (C_1, corresponding to the mid-summer temperature maximum or salinity minimum) had a significant positive temperature trend in the near surface in the NW region (Fig. 8, left panel), and a significant negative trend in salinity at the surface in the GoA and NW regions (Fig. 8, right panel). There were few significant trends in the phase term (φ_1) for temperature. There was a negative trend in salinity at the surface in the GoA region, and a positive trend in the top-most depth bins in in the NW region (Fig. 9, right panel). A trend of 0.025 rad corresponds to a time shift of just under 1.5 days, which indicates a shift of the annual salinity minima to earlier timing (about 1 week earlier over the course of the entire dataset) in the GoA region, and to a later timing (4–5 days) in the NW region.

Mixed layer depth anomalies over time indicated a shallowing trend in the depth of the seasonal thermocline in all but the E region (Fig. 10; negative anomalies imply a MLD thinner than average). The slopes of the anomalies suggest a shoaling of the seasonal pycnocline within PWS of slightly more than 3 m decade^{-1}. Although there were long-term trends, there was also considerable year-to-year variability, with several stanzas having similar mixed layer depths. There was no indication of consistent seasonal changes in MLD.

Temperatures were out of phase with the 18.6-year nodal tide (LNC) with a 4–5-year lag, with the strongest correlations ($r = 0.4–0.5$, $p < 0.05$) at depths greater than 100 m in all regions except E (Fig. 11). Because the LNC is an oscillation, the figures repeat on an 18.6-year cycle and the high positive correlations at long lags (13–14 years) are equivalent to a lead time of 4–5 years. Lagged correlations with salinity showed broadly similar patterns, although the correlations were not as strong (excepting the E region, with the lowest data density).

The PDO index lead temperatures in the top 200 m in all regions by 3–12 months, with longer leads in the deeper waters of the NW region (Fig. 12). Salinity was weakly correlated with the PDO at short time scales, though there were not consistent patterns among the regions. Cross correlations between NPGO and temperature also varied among the regions (Fig. 13), the strongest correlations were with temperature at depth at long lags in the NW region (and to a lesser degree the GoA region). Salinity was broadly positively correlated to NPGO at all depths in the GoA, and at 100–200 m in the CS and E regions. NPGO was not well correlated with salinity in the NW region.

The mechanisms driving PDO and NPGO might be related to the LNC, and a cross correlation was done between both indices and the LNC (not shown). NPGO was uncorrelated with the LNC ($p < 0.05$ at every lag), and PDO was weakly correlated, with significant ($p < 0.05$) correlation peaks of $r = -0.18$ and 0.18 at 23 and 135 months, respectively.

3.2. SST

SST trends varied among the regions, with a long-term slope that was not significantly different from zero in the CS and E regions (Fig. 14). There was a small but significant cooling trend in SST in the NW region (slope: − 0.09 °C decade^{-1}, 95% CI: − 0.017 to − 0.010) and a warming trend in the GoA region (slope: 0.08 °C decade^{-1}, 95% CI: 0.03–0.14).

3.3. Surface heat flux, upwelling, precipitation and discharge

Surface heat flux anomalies were primarily positive at the beginning of the time series, with a negative trend; positive anomalies became more prevalent in the late 1970s/early 1980s (Fig. 14). The NCEP convention of positive heat flux is from the ocean to the atmosphere was used, indicating an increase in heat flux to the surface ocean over

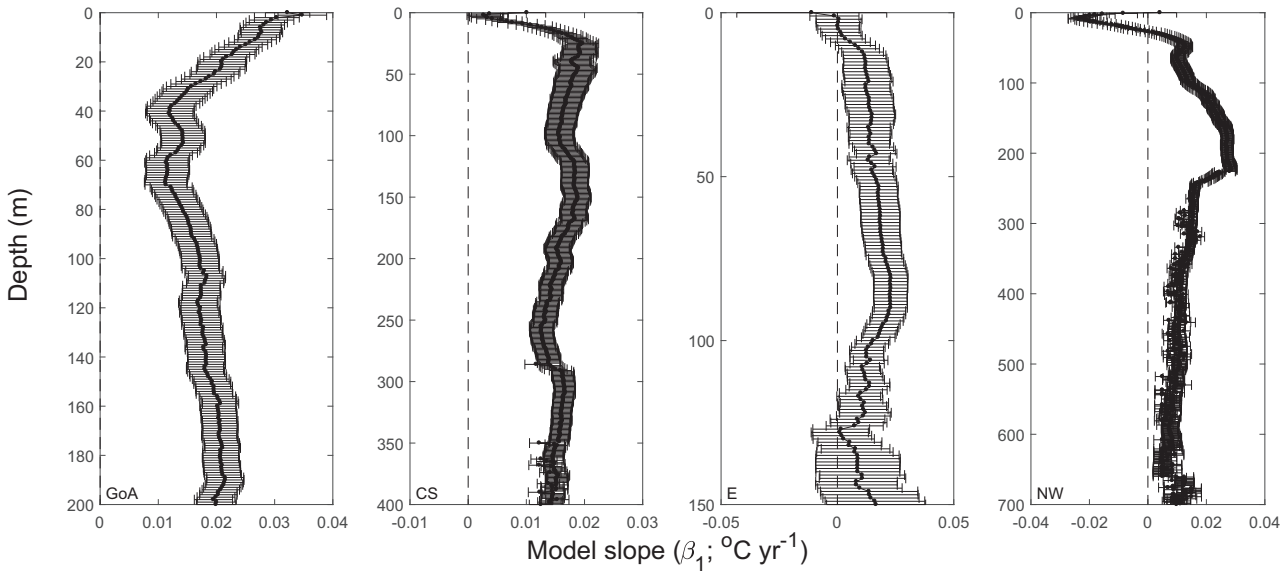

Fig. 5. Profiles of β_1 (i.e. the long term slope in Eq. (2)) fit to temperature, in the four Prince William Sound geographic regions (Fig. 1). Error bars indicate 95% confidence intervals for the parameter. Note that both axes change among figures.

time.

Upwelling index anomalies did not show a long-term trend on a monthly basis (the slope was not significantly different from zero), and did not exhibit significant 18.6-year periodicity (Fig. 14). Spectral analysis of the upwelling time series identified a main peak in the power spectral density at ~ 12 months, with a second smaller peak at ~ 6 months. An annual upwelling index, calculated as the sum of all the monthly anomalies in each calendar year, showed a significantly positive trend over time. Heat flux was positively correlated with the PDO (at lags up to 7 months) but not the NPGO; the upwelling index was not significantly correlated with the climate indices.

The precipitation and discharge time series were the best available but the shortest records employed in this analysis, beginning in 1979 (Fig. 15). There was no long-term trend in precipitation. There was a small but positive trend in discharge anomaly.

4. Discussion

4.1. High vs low frequency variability

The trends observed in this study were of much lower magnitude than the considerable inter- and intra-annual variability in temperature and salinity. There is no doubt considerable high frequency temporal and spatial variability in the region: Vaughan et al. (2001), for instance, highlighted the spatial and temporal variability in temperature and salinity in central PWS that is caused by smaller scale oceanographic processes (and all the data used by Vaughan et al., 2001 is included in this study). This type of analysis cannot account for that high frequency variability, and it is assumed that the considerable variability surrounds the mean. Most prior work in the North Pacific has been from a small number of regularly visited stations (e.g. Royer, 1993; Royer and Grosch, 2006; Royer et al., 2001), but there has not been a similar coordinated effort undertaken in the PWS region. It can be expected

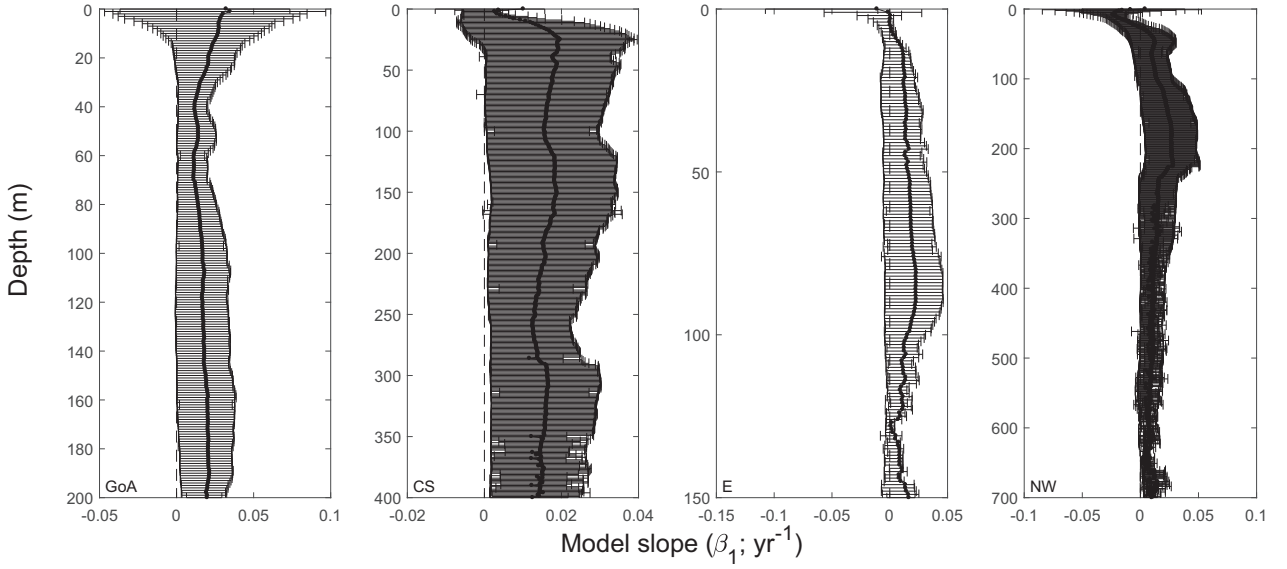

Fig. 6. Profiles of β_1 (i.e. the long term slope in Eq. (2)) fit to salinity, in the four Prince William Sound geographic regions. Error bars indicate 95% confidence intervals for the parameter. Note that both axes change among figures.

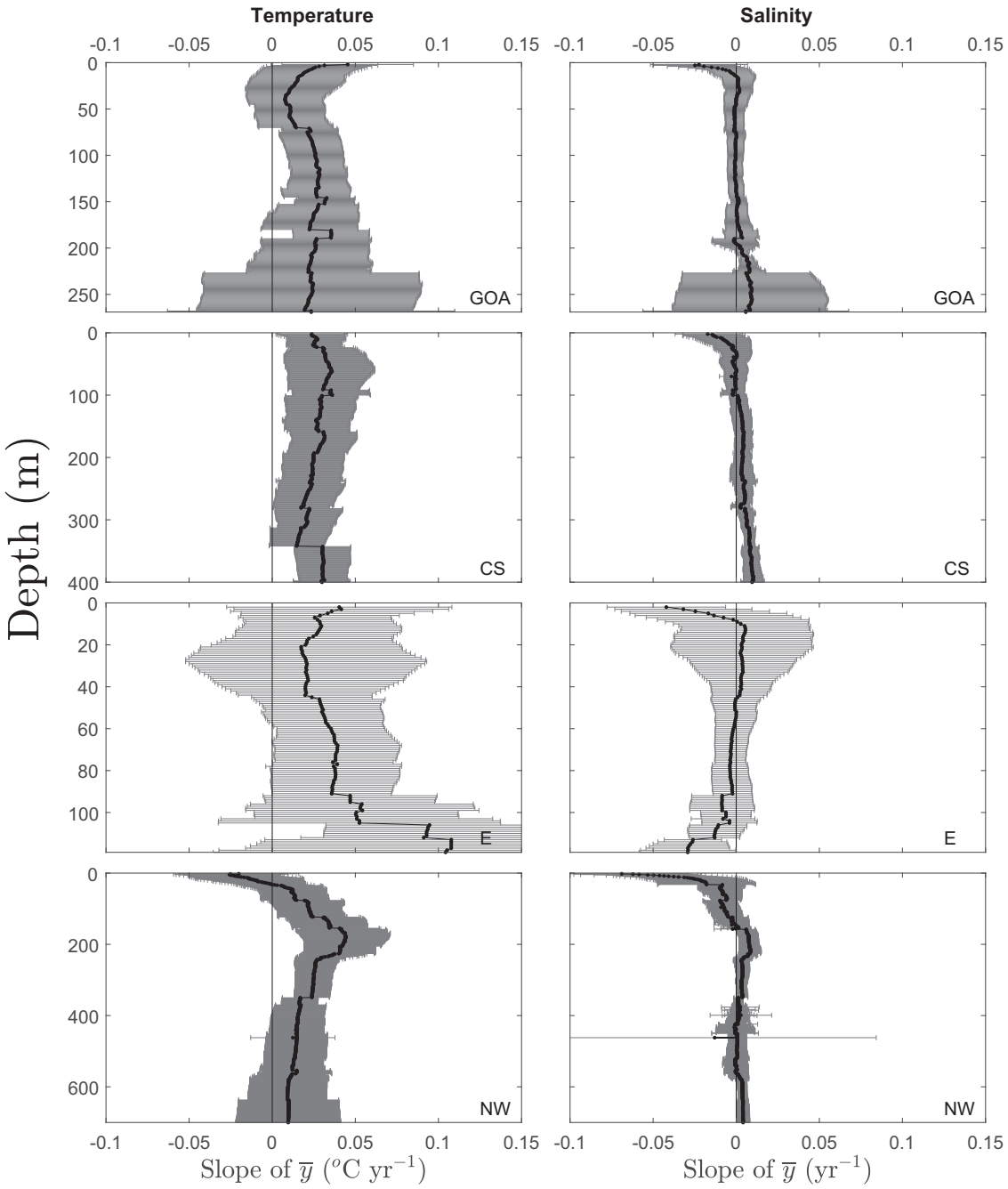

Fig. 7. Profiles of the slope of $\bar{y}$ ("annual mean") over time in the four Prince William Sound geographic regions (Fig. 1) for temperature (left panel) and salinity (right panel). Bars indicate 95% confidence intervals. Note that the scaling of the ordinate differs among regions.

that using ensembles of stations in this way will increase the likelihood of type II errors and will therefore likely fail to detect some existing patterns. For this reason, several complementary methods and models were used, but they did not always agree, leading to some ambiguity in the interpretations.

4.2. Climatological annual cycles

The climatological annual cycle that emerges from this analysis is similar from region to region and similar to that of Xiong and Royer (1984): following winter minima in February-April, surface temperatures begin to warm in May, with warming largely confined to the upper 25 m of the water column (Fig. 3). The thermocline begins to break down in September and heat is mixed downward into the water column. The salinity cycle is similar, with surface salinity beginning to decrease in late May, decreasing over the summer, and being mixed downward in autumn (Fig. 3). Salinity also tends to increase at depth during the summer months (June–Sept), as deep-water renewal occurs. Halverson et al. (2012) observed annual renewal events at moorings in Hinchinbrook Entrance during that same time between 2005 and 2010.

The MLD climatology presented here (Fig. 4) also matches the canonical pattern for the region described previously (Henson, 2007; Musgrave et al., 2013; Weingartner, 2007). MLD was deepest in offshore locations (GoA and CS) in autumn/winter and shoaled in spring. More protected locations (E and NW) experienced an earlier return to stability and retained a shallower MLD longer into autumn, as would be expected from enhanced stability from near shore freshwater inputs and comparatively less wind mixing in protected locations with less fetch.

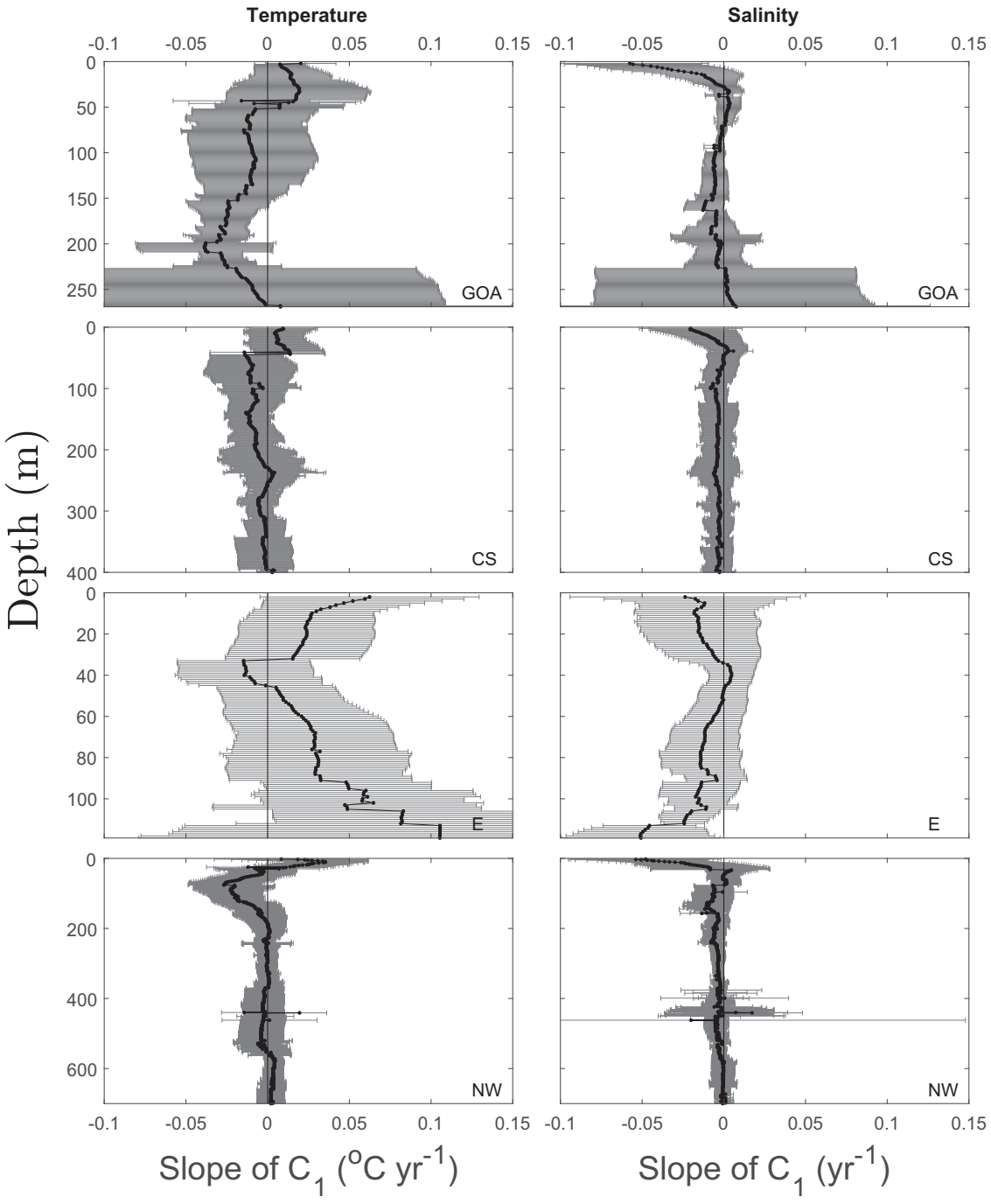

Fig. 8. Profiles of the slope of C_1 (amplitude) over time in the four Prince William Sound geographic regions (Fig. 1) for temperature (left panel) and salinity (right panel). Bars indicate 95% confidence intervals. Note that the scaling of the ordinate differs among regions.

On the shelf adjacent to PWS, latent and sensible heat fluxes were on average a net loss from the ocean to the atmosphere (Fig. 4), with the highest fluxes in winter, as is to be expected for the region (Janout et al., 2010; Bond et al., 2015). The upwelling index climatology (Fig. 4) showed weak upwelling in the summer, peaking in June/July and coinciding with the increase in salinity at depth (Fig. 3) likely caused by deep-water renewal (Halverson et al., 2012). Downwelling predominated during the winter months.

4.3. Long term trends in the PWS region

In the waters adjacent to PWS (GoA), there was a warming trend in the last 40 years of ~ 0.2 to 0.3 °C per decade, with most warming at the surface (Figs. 5, 7 and 14), similar to the trends observed as part of a larger pattern of warming throughout the region (Royer and Grosch, 2006; Wu and Li, 2007). Beyond an overall increase in temperature, the annual model fits did not suggest any meaningful changes in the magnitude of the annual peak or in timing.

At depth (> 150 m), there was a decrease in the amplitude of the annual temperature maximum (Fig. 8). The freshening trend observed by Royer and Grosch (2006) at the GAK1 site off Seward, AK was less evident in the shelf region (GoA) included here, but their site, in the mouth of Resurrection Bay, was nearshore and downstream of PWS and may have thus reflected, in part, the outflows from NW PWS (as well as the rest of the coastal margin upstream of Resurrection Bay). A freshening trend at the surface from the annual analysis of casts occurred

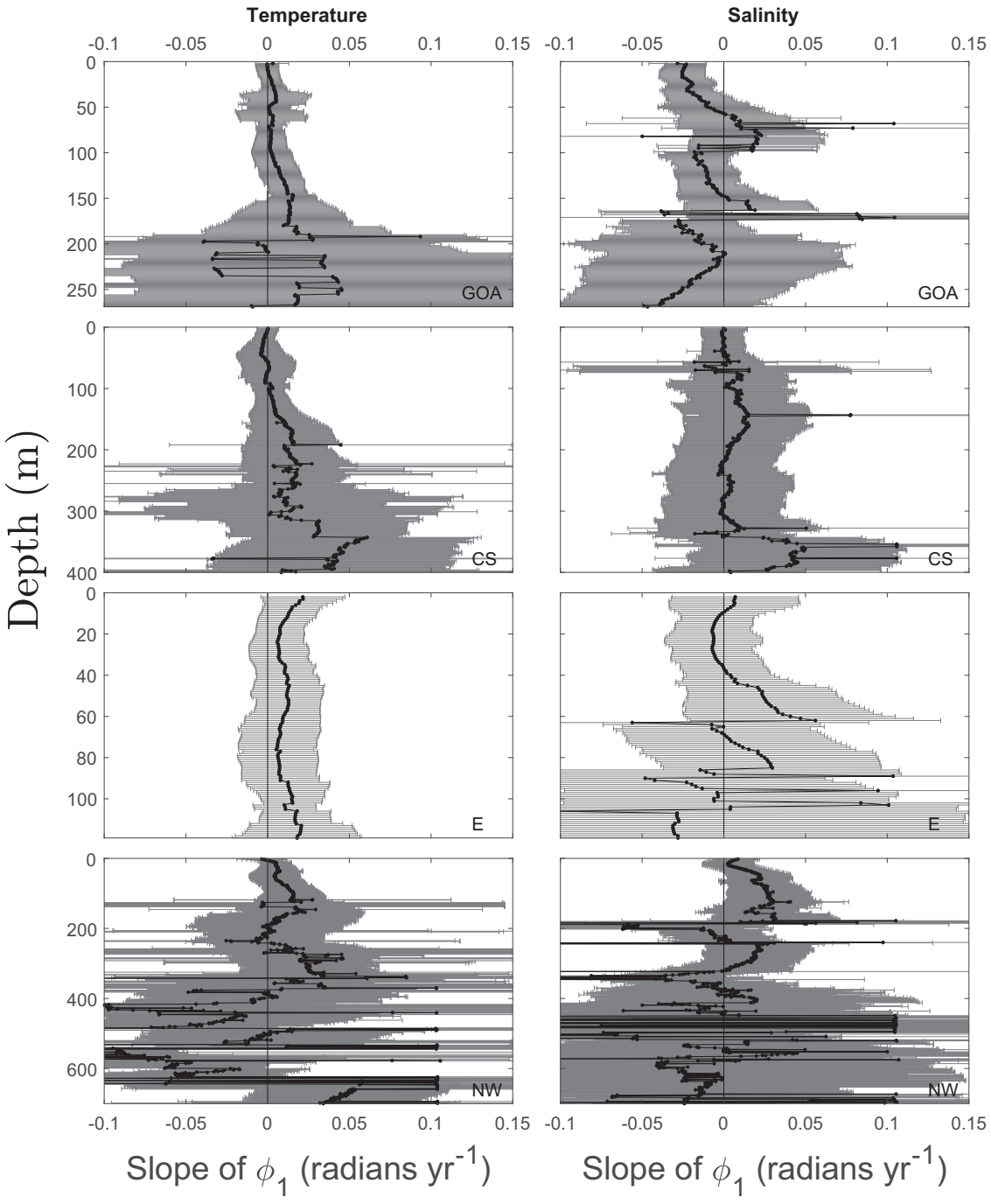

Fig. 9. Profiles of the slope of φ_1 (phase) over time in the four Prince William Sound geographic regions (Fig. 1) for temperature (left panel) and salinity (right panel). Bars indicate 95% confidence intervals. Note that the scaling of the ordinate differs among regions.

near surface in the NW region (Fig. 6), but with a trend towards higher salinities at depth. These observations suggest an enhancement in deep-water renewal events over time, with more cool, salty water transported shoreward during the deep-water renewal season, which could account for the observed reduction in the annual maximum. An enhancement in deep-water renewal could also be expected to accompany decreases in surface runoff because enhanced surface transport will cause entrainment of more saline water at depth (Royer, 2005; see below).

In central PWS there was also a warming trend of similar magnitude to GoA at most depths identified by both the simple and annual regression models, there was again no evidence for changes in timing or the magnitude of the summer maximum. Trends in salinity were similar to the GoA region, with an increase at depth and non-significant increase at the surface. The interpretation for those trends is essentially the same as the GoA region: PWS may be considered to be a large estuary (e.g. Vaughan et al., 2001), and enhanced outflowing freshwater fluxes at the surface can be expected to increase entrainment and be compensated by inflowing higher salinity water at depth (see below). The eastern portion of PWS (area E) also generally showed the same trends, although they were less likely to be detectable (i.e. significantly different from zero), presumably due to the comparatively lower data density there (rather than combining the region with CS, it has been left separate to preserve the regions used by Musgrave et al., 2013).

In northwestern PWS, the simple regression model showed declining temperatures near surface and a warming trend at depth; annual regressions had a similar pattern in annual mean temperature near

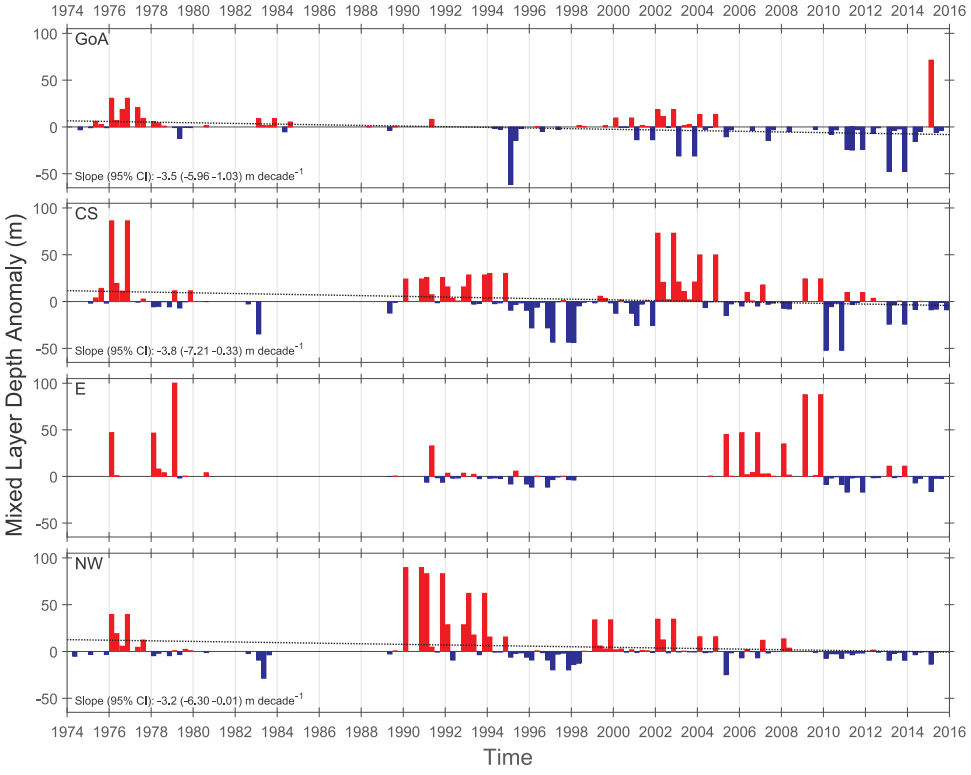

Fig. 10. Quarterly averages of the mixed layer depth (MLD) anomaly time series in the four Prince William Sound geographic regions (Fig. 1). Long term slopes are only reported for regions where the slope of the line was significantly different from zero.

surface, but the 95% CI spanned zero (Fig. 7). There was also a negative trend in the annual maximum temperature parameter (C_1; Fig. 8), which suggests that the annual temperature maximum has been declining in that region (both overall, and in terms of the maximum temperature reached). Annual regressions (which are more conservative, since years with few observations are dropped) also found a non-significant negative trend in annual mean temperature

There was also a trend towards declining salinity at the surface in the NW region, but no significant trend at depth (Fig. 6, Fig. 7). The overall picture suggests a general cooling and freshening at the surface, and warming and increasing salinity trends at depth. A freshening trend can be the result of enhanced inputs of freshwater through precipitation and/or runoff, and a cooling trend will be the result of reduced surface heat flux or transport. The estimates of heat flux from the adjacent shelf suggest that surface fluxes from the atmosphere to the ocean have been increasing in the region (Fig. 14).

The hydrologic connections between the atmosphere, land, and surface ocean in Prince William Sound are not well described. The region is poorly gaged, has sparse weather observations, and consists of numerous small watersheds (e.g. see Beamer et al., 2016). Precipitation in the region is considerable (Shulski and Wendler, 2008), but earlier hydrological models (Royer, 1982; Royer, 2005; Wang, 2004; Hill et al., 2015) did not show long-term trends in discharge. The available precipitation and discharge estimates used here suggest that precipitation has not changed significantly in the region in recent decades, while there has been a modest increase in discharge. Recent estimates of ice mass in the GoA region suggest a negative mass balance in the region (Arendt et al., 2013), and declines in watershed storage (Hill et al., 2015; Beamer et al., 2016), and that discharge may thus represent freshwater derived from ice storage. Most of the ice mass in PWS is concentrated on the western side (i.e. the NW region, Fig. 1), and the freshening trend observed there may reflect inputs from ice ablation. The Beamer et al. (2016) discharge estimates do not include inputs from tidewater glaciers (which are also largely receding in the PWS region, e.g. Colgan et al., 2012) that represent another potential source of freshwater and negative heat inputs.

The cooling and freshening trend near surface in the NW region thus could be the combination of two mechanisms: At the surface (~ 0 to 10 m, the depth of the seasonal thermocline: Fig. 4), increased discharge of freshwater of glacial origin would lead to reductions in the average temperature and salinity. The increased discharge would also increase entrainment of deep water (generally cooler and more saline than surface water). The resulting circulation of cool deep water towards the surface would then be responsible for the reduction of temperature just below the surface layer, to a depth of ~ 30 m (Fig. 5). At depths well away from the surface layer, salinity has increased over time, which is most likely a reflection of the overall enhanced movement of deep water into PWS from the shelf.

Exchange between PWS and the adjacent shelf is primarily northward through Hinchinbrook Entrance (Niebauer et al., 1994; Halverson et al., 2012) and is driven in part by wind (Niebauer et al., 1994). In winter, westward winds drive near-surface transport, and in summer and autumn the relaxing of wind driven downwelling allows a flux of slope water along the bottom into the basins of PWS (Ladd et al., 2005; Weingartner et al., 2005). The upwelling anomaly index used here (Fig. 14) is a proxy for that transport (Halverson et al., 2012). The northern GoA shelf is a primarily downwelling system, upwelling is generally weak at best (Stabeno et al., 2004; Halverson et al., 2012). The positive trend in “upwelling” observed here on the shelf (Fig. 14) is thus best viewed as a reduction in downwelling, rather than increased upwelling: most of the positive upwelling anomalies, particularly since the 1990s, occurred during the winter months, when downwelling predominates (Fig. 4). Reduced downwelling would tend to lead to enhanced deep-water renewal during late summer/autumn. That is also the time of maximal freshwater inputs to the surface (Fig. 3) and when entrainment could be expected to be highest as well.

4.4. Long term changes attributable to large scale drivers

Several long-term trends and oscillations have been identified in the North Pacific at varying time scales, from 50 to 70 years (Minobe, 1997), 23 years (Gedalof and Smith, 2001), the 18.6-year lunar nodal

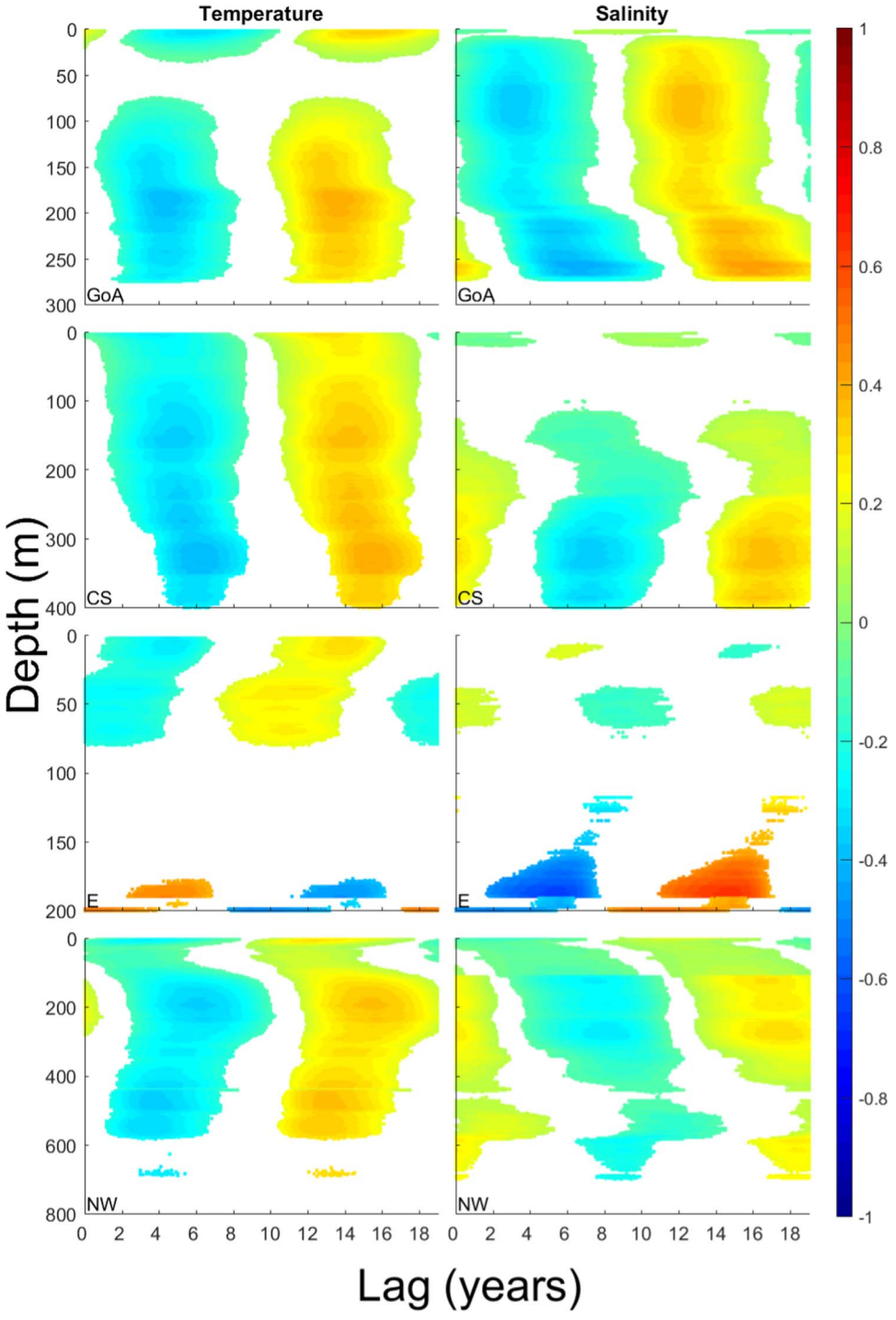

Fig. 11. Cross correlations (lags only) between the Lunar Nodal Cycle (LNC) and temperature (left panels) and salinity (right panels) in the four Prince William Sound geographic regions (Fig. 1). Note that the scaling of the ordinate differs among regions. Only significant correlations ($p < 0.05$, from 10,000 simulated probability distribution functions) are shown.

tide (Royer, 1993) and quasi-decadal (Mantua et al., 1997; Di Lorenzo et al., 2008); this analysis has focused on the latter three, given the length of the time series. There was some correspondence between conditions in PWS and the North Pacific in general terms: there was a switch from cool to warm SST in 1977 (Fig. 14, top panel), which corresponds to the basin-wide regime shift that occurred around that time (Hare and Mantua, 2000), although SST did not stay positive into the 1980s in PWS as they did elsewhere. Negative surface heat flux anomalies became more prominent at approximately the same time (Fig. 14). PWS also experienced a cool phase beginning in 2006 that corresponds to the cool period identified on the GoA shelf off Seward, Alaska (Janout et al., 2010), and switched toward positive anomalies in late 2013, as did the central GoA (the “Blob” anomaly of Bond et al., 2015). Both of those contemporary stanzas appear to have been in part due to winter cooling processes (which are varied and complex, e.g. Janout et al., 2010), which manifested immediately south of PWS as well: the upwelling anomaly (Fig. 14, bottom panel) suggests that winter winds were strongly downwelling in 2006–2007, and less so from 2011 onward.

The PDO is the first principal component of SST in the North Pacific (Mantua et al., 1997), and is also correlated with sea surface height (Di Lorenzo et al., 2008), it describes the dominant spatial and temporal patterns of SST in the northeastern Pacific Ocean. The PDO pattern is not a monolithic climatic mode, it is the sum of several drivers including variations in surface heat flux and wind-driven transport, oceanic thermal inertia, and decadal variations in the Oyashio/

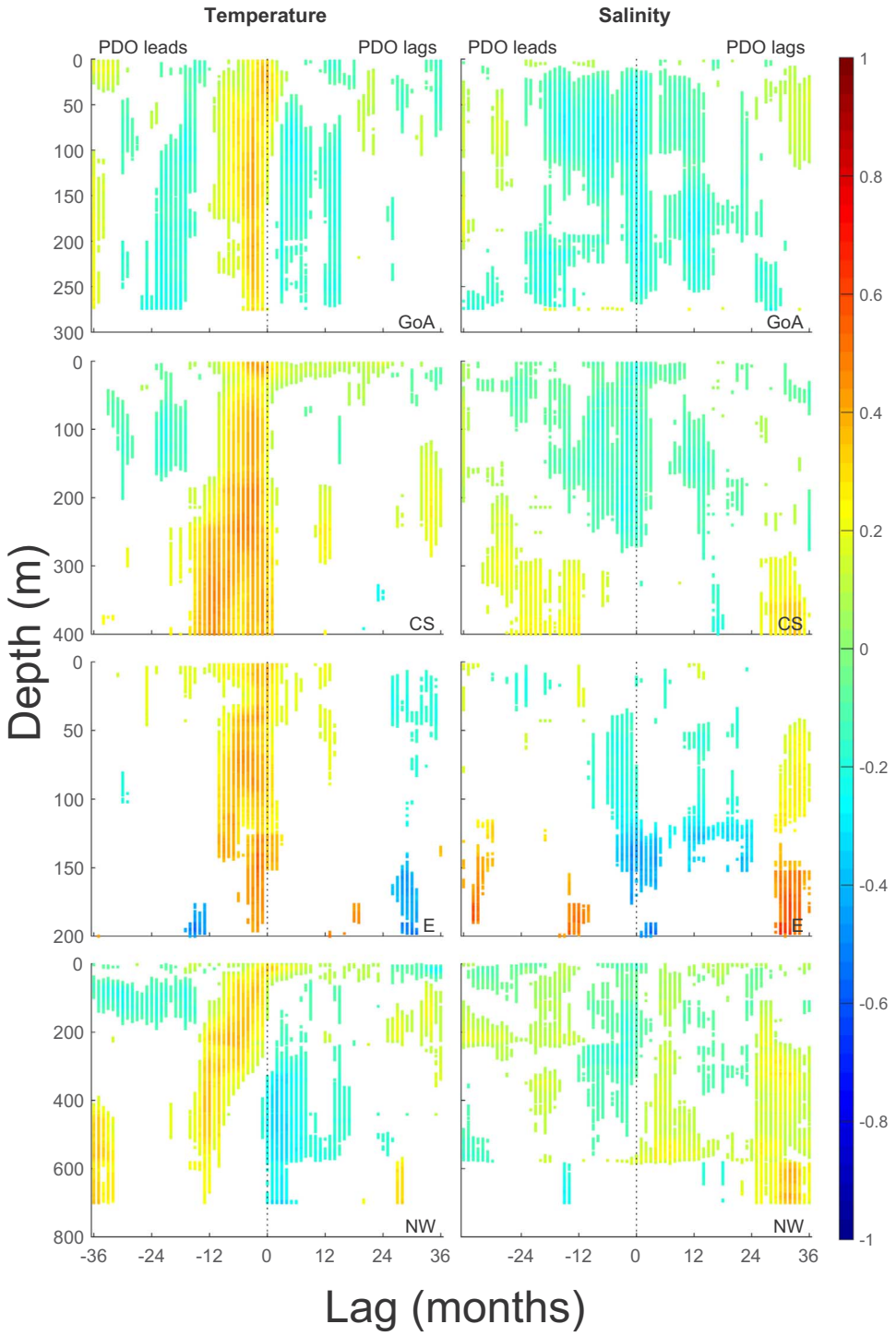

Fig. 12. Cross correlations between the Pacific Decadal Oscillation (PDO) and temperature (left panels) and salinity (right panels) in the four Prince William Sound geographic regions (Fig. 1). Note that the scaling of the ordinate differs among regions. Only significant correlations ($p < 0.05$, from 10,000 simulated probability distribution functions) are shown.

Kuroshio extension (Newman et al., 2016). The PDO pattern also reflects variability driven by the El Niño Southern Oscillation (ENSO) and correlates with ENSO indices. The NPGO is the second principal component of sea surface height, and reflects changes in geostrophic circulations in the North Pacific; a positive NPGO is associated with a strengthening of the Alaska Current (Di Lorenzo et al., 2008).

Cross correlations of the PDO and NPGO with temperature and salinity highlight the connections between large-scale patterns in the Gulf of Alaska and PWS. Temperature at most depths lagged the PDO (Fig. 12), presumably caused by lags attributable to transport time and mixing. Salinity also lagged the NPGO (Fig. 13) and was correlated at much broader temporal ranges, perhaps reflecting the longer-term changes in circulation (indexed by the NPGO) versus shorter term atmospheric variability (indexed in part by the PDO). Flushing times of PWS vary seasonally, with a minimum in summer (> 500 days) and maximum in autumn/winter (120–300 days: Niebauer et al., 1994; Halverson, 2012) and vary by depth (e.g. most transport during summer months is at depth). The relatively long lags of NPGO relative to salinity may also reflect long-term oscillations. Although the correlations indicate that the indexes account for a relatively small proportion of the variance, they are consistent with correlations done at regional scales (Di Lorenzo et al., 2008; Newman et al., 2016).

An 18.6-year periodicity is a common feature of geophysical time series of adequate length (Currie, 1996) and has been observed in SST

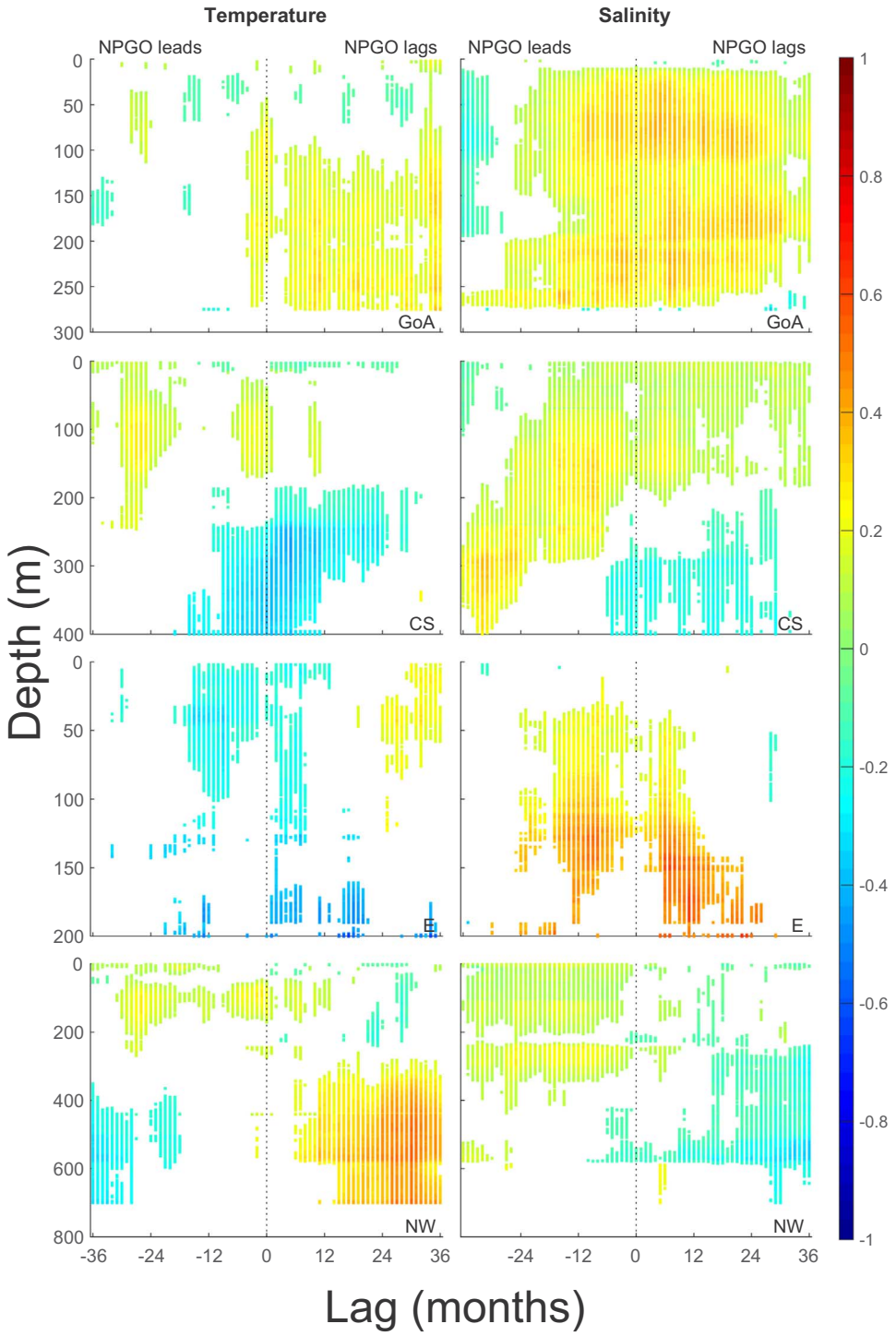

Fig. 13. Cross correlations between the North Pacific Gyre Oscillation (NPGO) and temperature (left panels) and salinity (right panels) in the four Prince William Sound geographic regions (Fig. 1). Note that the scaling of the ordinate differs among regions. Only significant correlations ($p < 0.05$, from 10,000 simulated probability distribution functions) are shown.

records from coastal Alaska (Royer, 1993) and British Columbia (Loder and Garrett, 1978; McKinnell and Crawford, 2007). The mechanisms by which the lunar declination cycle alter surface temperature are unclear, it has been hypothesized that changes in tidal mixing or ocean-atmosphere heat flux are responsible (Loder and Garrett, 1978; McKinnell and Crawford, 2007). The latter authors used SST data from British Columbia and noted a two-year lag correlation between the LNC signal and the Pacific North America teleconnection index, which is an indicator of low-frequency variability in atmospheric circulation in the North Pacific (Barnston and Livezey, 1987). This suggests that the effect is likely part of much larger circulation patterns in the hemisphere (the cross-correlation pattern between temperature and the PNA index in the data used here was very similar to the PDO index, but correlation coefficients were lower). The lag observed here was of similar magnitude.

Cross correlations with profile data showed the LNC leading temperature and salinity by 4–5 years and that temperature and salinity patterns were broadly similar. Coupling with temperature near surface would tend to support the notion that atmospheric forcing is, in part, responsible for the oscillation, but correlation at depth and with salinity would also tend to implicate mixing processes. A weak but significant correlation between the LNC and PDO suggests a possible atmospheric link. However, the independence between NPGO and the LNC, but with significant cross correlations between salinity and the LNC, suggests

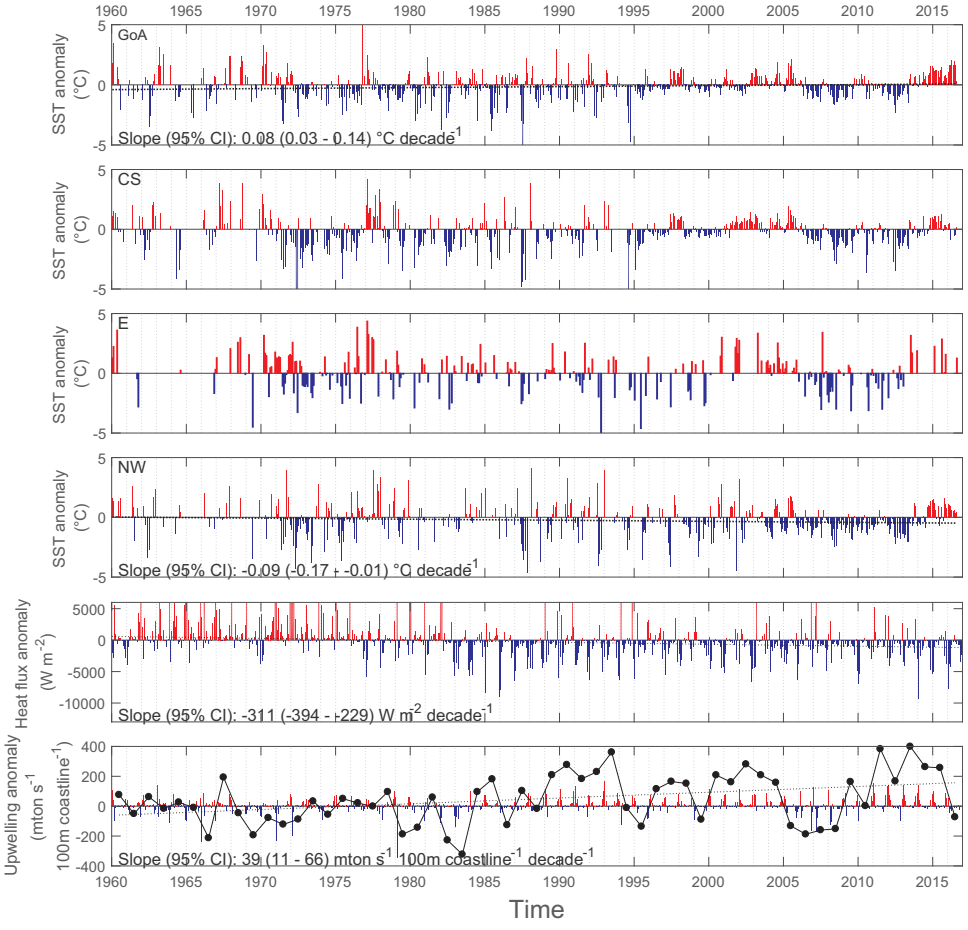

Fig. 14. Top four panels: Monthly average SST anomaly in the Prince William Sound regions (Fig. 1). Fifth panel: Heat flux anomaly (latent + sensible heat flux) at NCEP reanalysis point at 60°N 146°15′W (see text). The dashed line is the long-term trend fit by linear regression, slope and 95% CI are shown. Bottom panel: NOAA PFEL Upwelling anomaly (offshore component only) at 60°N 146°W. Bars are monthly anomalies and solid line and points are annual sums of anomalies (see text). The dashed line indicates the long-term trend of annual anomalies and the text indicates the slope and 95% CI.

two modes of salinity variability in the region, related to transport (NPGO) and mixing (LNC).

5. Conclusions

The overall picture that emerges from the data assembled here is a regional warming trend, with indications of enhanced freshwater inputs at the surface that in some regions are accompanied by a reduction in temperature attributable to inputs from melting ice. As well as generally higher average temperatures, there was a trend towards higher maximum temperatures during the summer maximum, but little in the way of changes in timing. At depth, the trend was towards warmer and more saline water, which is consistent with increased entrainment of deep water caused by enhanced surface circulation and deep-water transport. Both trends can be expected to enhance stability in near-surface waters, which can be seen by the shoaling of the seasonal mixed layer by several meters during the 40-year span examined here. Annual productivity is controlled in part by the timing and depth of the onset of stratification in spring (e.g. Sverdrup, 1953), and reductions in the depth of the seasonal mixed layer may result in reductions in overall seasonal productivity that may cascade in unpredictable ways to higher trophic levels (e.g. Benson and Trites, 2002).

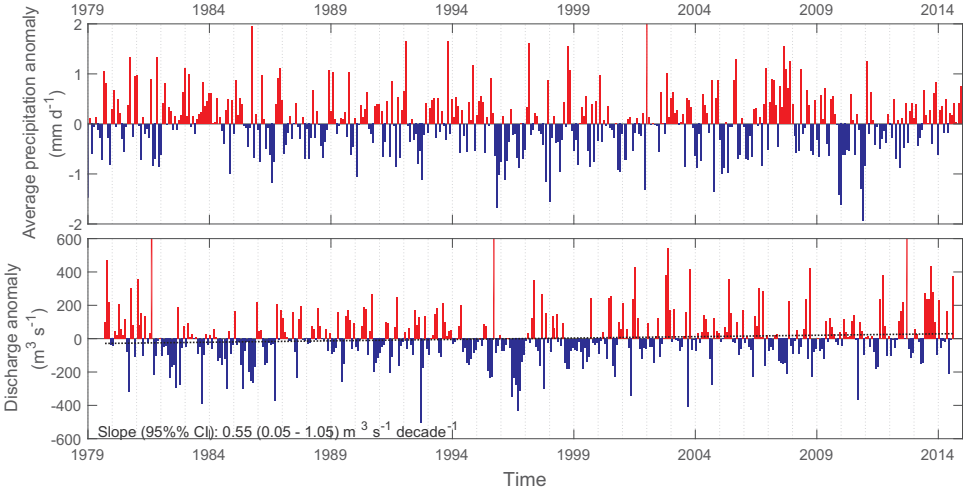

Fig. 15. Top panel: CMAP precipitation anomaly time series in the PWS region (1979–2015). Bottom panel: Discharge anomaly time series in the PWS region (i.e. along the periphery of PWS), from Beamer et al. (2016).

Acknowledgements

The research described in this paper was supported by the Exxon Valdez Oil Spill Trustee Council (Project 12120114-E). However, the findings and conclusions presented by the author are his own and do not necessarily reflect the views or position of the Trustee Council.

References

Arendt, A., Luthcke, S., Gardner, A., O'Neel, S., Hill, D., Moholdt, G., et al., 2013. Analysis of a GRACE glocal mascon solution for Gulf of Alaska glaciers. J. Glaciol. 59, 913–924. http://dx.doi.org/10.3189/2013JoG12J197.

Barclay, D.J., Yager, E.M., Graves, J., Kloczko, M., Calkin, P.E., 2013. Late Holocene glacial history of the Copper river Delta, coastal south-central Alaska, and controls on valley glacier fluctuations. Quat. Sci. Rev. 81, 74–89.

Barnett, T., Pierce, D.W., AchutaRao, K.M., Gleckler, P.J., Santer, B.D., Gregory, J.M., et al., 2005. Penetration of human-induced warming into the world's oceans. Science 309, 284–287.

Barnston, A.G., Livezey, R.E., 1987. Classification, seasonality and persistence of low-frequency atmospheric circulation patterns. Mon. Weather Rev. 115, 1083–1126.

Beamer, J.P., Hill, D.F., Arendt, A., Liston, G.E., 2016. High-resolution modeling of coastal freshwater discharge and glacier mass balance in the Gulf of Alaska watershed. Water Resour. Res. 52, 3888–3909. http://dx.doi.org/10.1002/2015WR018457.

Benson, A.J., Trites, A.W., 2002. Ecological effects of regime shifts in the Bering Sea and eastern North Pacific Ocean. Fish. Fish. 3, 95–113.

Bond, N.A., Cronin, M.F., Freeland, H., Mantua, N., 2015. Causes and impacts of the 2014 warm anomaly in the NE Pacific. Geophys. Res. Lett. 42, 3414–3420. http://dx.doi.org/10.1002/2015GL063306.

Branch, M.A., Coleman, T.F., Li, Y., 1999. A Subspace,interior, and conjugate gradient method for large-scale bound-constrained minimization problems. SIAM J. Sci. Comput. 21, 1–23.

Colgan, W., Pfeffer, W.T., Rajaram, H., Abdalati, W., Balog, J., 2012. Monte Carlo ice flow modeling projects a new stable configuration for Columbia Glacier, Alaska, c. 2020. Cryosphere 6, 1395–1409. http://dx.doi.org/10.5194/tc-6-1395-2012. (2012).

Currie, R.G., 1996. Variance contribution of luni-solar (Mn) and solar cycle (Sc) signals to climate data. Int. J. Climatol. 16, 1343–1364.

Doodson, A.T., 1921. The harmonic development of the tide-generating potential. Proc. R. Soc. Lond. A 100, 305–329.

Di Lorenzo, E., Schneider, N., Cobb, K.M., Chhak, K., Franks, P.J.S., Miller, A.J., et al., 2008. North Pacific Gyre Oscillation links ocean climate and ecosystem change. Geophys. Res. Lett. 35, L08607. http://dx.doi.org/10.1029/2007GL032838.

Fairall, C.W., Bradley, E.F., Rogers, D.P., Edson, J.B., Young, G.S., 1996. Bulk parameterization of air-sea fluxes for tropical ocean-global atmosphere coupled-ocean atmosphere response experiment. J. Geophys. Res. 101, 3747–3764.

Feeley, R.A., 1979. Processes affecting the distribution and transport of suspended matter in the northeast Gulf of Alaska. Deep Sea Res. 26, 445–464.

Gay, S.M., Vaughan, S.L., 2001. Seasonal hydrography and tidal currents of bays and fjords in Prince William Sound, Alaska. Fish. Oceanogr. 10 (Suppl. 1), S159–S193.

Gedalof, Z., Smith, D.J., 2001. Interdecadal climate variability and regime-scale shifts in Pacific North America. Geophys. Res. Lett. 24, 1515–1518.

Hare, S.R., Mantua, N., 2000. Empirical evidence for North Pacific regime shifts in 1977 and 1989. Prog. Oceangr. 47, 103–145.

Halverson, M.J., Belanger, C., Gay, S.M., 2012. Seasonal variations in the transport through the straits connecting Prince William Sound to the Gulf of Alaska. Cont. Shelf Res. http://dx.doi.org/10.1016/j.csr.2012.06.017.

Henson, S.A., 2007. Water column stability and spring bloom dynamics in the Gulf of Alaska. J. Mar. Res. 65, 715–736.

Hill, D.F., Bruhis, N., Calos, S.E., Arendt, A., Beamer, J., 2015. Spatial and temporal variability of freshwater discharge into the Gulf of Alaska. J. Geophys. Res. 120, 634–646. http://dx.doi.org/10.1002/2014JC010395.

Janout, M.A., Weingartner, T.J., Royer, T., Danielson, S.L., 2010. On the nature of winter cooling and the recent temperature shift on the northern Gulf of Alaska shelf. J. Geophys. Res. 115, C05023. http://dx.doi.org/10.1029/2009JC005774.

Kalnay, E., Kanamitsu, M., Kistler, R., Collins, W., Deaven, D., Gandin, F., et al., 1996. The NCEP/NCAR 40-year reanalysis project. Bull. Am. Met. Soc. 77, 437–471.

Ladd, C., Stabeno, P., Cokelet, E.D., 2005. A note on cross-shelf exchange in the northern Gulf of Alaska. Deep Sea Res. II 52, 667–669. http://dx.doi.org/10.1016/j.dsr2.2004.12.022.

Levitus, S.J., Antonov, J.I., Wang, J., Delworth, T.L., Dixon, K.W., Broccoli, A.J., 2001. Anthropogenic warming of Earth's climate system. Science 292, 267–270.

Li, M., Myers, P.G., Freeland, H., 2005. An examination of historical mixed layer depths along Line P in the Gulf of Alaska. Geophys. Res. Lett. 32, L05613. http://dx.doi.org/10.1029/2004GL021911.

Loder, J.W., Garrett, C., 1978. The 18.6-year cycle of sea surface temperature in shallow seas due to tidal mixing. J. Geophys. Res. 83, 1967–1970.

Mantua, N.J., Hare, S.R., Zhang, Y., Wallace, J.M., Francis, R.C., 1997. A Pacific interdecadal climate oscillation with impacts on salmon production. Bull. Am. Meteorol. Soc. 78, 1069–1079. http://dx.doi.org/10.1175/1520-0477(1997)078,1069:APICOW.2.0.CO;2.

McKinnell, S.M., Crawford, W.R., 2007. The 18.6-year lunar nodal cycle and surface temperature variability in the northeast Pacific. J. Geophys. Res. 112, C02002. http://dx.doi.org/10.1029/2006JC003671.

Minobe, S., 1997. A 50-70 year climatic oscillation over the North Pacific and North America. Geophys. Res. Lett. 24, 683–686.

Musgrave, D.L., Halverson, M.J., Pegau, W.S., 2013. Seasonal surface circulation, temperature, and salinity in Prince William Sound, Alaska. Cont. Shelf Res. 53, 20–29.

National Centers for Environmental Information/NESDIS/NOAA/U.S. Department of Commerce, Research Data Archive/Computational and Information Systems Laboratory/National Center for Atmospheric Research/University Corporation for Atmospheric Research, Earth System Research Laboratory/NOAA/U.S. Department of Commerce, Cooperative Institute for Research in Environmental Sciences/University of Colorado, National Oceanography Centre/Natural Environment Research Council/United Kingdom, Met Office/Ministry of Defence/United Kingdom, Deutscher Wetterdienst (German Meteorological Service)/Germany, Department of Atmospheric Science/University of Washington, and Center for Ocean-Atmospheric Prediction Studies/Florida State University., 2016, updated monthly. International Comprehensive Ocean-Atmosphere Data Set (ICOADS) Release 3, Individual Observations. Research Data Archive at the National Center for Atmospheric Research, Computational and Information SystemsLaboratory. ⟨http://dx.doi.org/10.5065/D6ZS2TR3⟩ (Accessed 20 September 2016).

Neal, E.G., Hood, E., Smikrud, K., 2010. Contribution of glacier runoff to freshwater discharge into the Gulf of Alaska. Geophys. Res. Lett. 37, L06404. http://dx.doi.org/10.1029/2010GL042385.

Newman, M., Alexander, M.A., Ault, T.R., Cobb, K.M., Deser, C., Di Lorenzo, E., et al., 2016. The pacific decadal oscillation, revisited. J. Climate 29, 4399–4427.

Niebauer, H.J., Royer, T.C., Weingartner, T.J., 1994. Circulation of Prince William Sound, Alaska. J. Geophys. Res. 99, 14113–14126.

NOAA.El Niño/Southern Oscillation (ENSO) Diagnostic Discussion. Available: ⟨http://www.cpc.ncep.noaa.gov/products/analysis_monitoring/enso_disc_jan2016/ensodisc.pdf⟩.

Royer, T.C., 1982. Coastal fresh water discharge in the Northeast Pacific. J. Geophys. Res. 87, 2017–2021.

Royer, T.C., 1993. High latitude oceanic variability associated with the 18.6-year nodal tide. J. Geophys. Res. 98, 4639–4644.

Royer, T.C., 2005. Hydrographic responses at a coastal site in the northern Gulf of Alaska to seasonal and interannual forcing. Deep. Res. II 52, 267–288.

Royer, T.C., Grosch, C.E., 2006. Ocean warming and freshening in the northern Gulf of Alaska. Geophys. Res. Lett. 33, L16605. http://dx.doi.org/10.1029/2006GL026767.

Royer, T.,C., Grosch, C.E., Mysak, L.A., 2001. Interdecadal variability of Northeast Pacific coastal freshwater and its implications on biological productivity. Prog. Oceanogr. 49, 95–111.

Sarkar, N., Royer, T.C., Grosch, C.E., 2005. Hydrographic and mixed layer depth variability on the shelf in the northern Gulf of Alaska, 1974–1998. Cont. Shelf Res. 25, 2147–2162.

Stabeno, P.J., Bond, N.A., Hermann, A.J., Kachel, N.B., Mordy, C.W., Overland, J.E., 2004. Meteorology and oceanography of the Northern Gulf of Alaska. Cont. Shelf Res. 24, 859–897.

Shulski, M., Wendler, G., 2008. The Climate of Alaska. University of Alaska Press, Fairbanks, pp. 216.

Sverdrup, H.U., 1953. On conditions for the vernal blooming of phytoplankton. J. Cons. Int. Explor. Mer. 18, 287–295.

Thomson, R.E., Fine, I.V., 2003. Estimating mixed layer depth from oceanic profile data. J. Atmos. Ocean. Tech. 20, 319–329.

Vaughan, S.L., Mooers, C.N.K., Gay, S.M., 2001. Physical variability in Prince William Sound during the SEA Study (1994–98). Fish. Oceanogr. 10 (Suppl. 1), 58–80.

Wang, J., Jin, M., Patrick, V., Allen, J.R., Eslinger, D.L., Mooers, C.N., et al., 2001. Numerical simulations of the seasonal circulation patterns and thermohaline structures of Prince William Sound, Alaska. Fish. Oceanogr. 10 (Suppl. 1), 132–148.

Wang, J., Jin, M., Musgrave, D., Ikeda, M., 2004. A hydrological digital elevation model for freshwater discharge into the Gulf of Alaska. J. Geophys. Res. 109, C07009. http://dx.doi.org/10.1029/2002JC001430.

Weingartner, T., 2007. Atmosphere and ocean. In: Spies, R.B. (Ed.), Long Term Ecological Change in the Gulf of Alaska. Elsevier B.V, Amsterdam, pp. 266–273.

Weingartner, T.J., Danielson, S.L., Royer, T.C., 2005. Freshwater variability and predictability in the Alaska Coastal Current. Deep Sea Res. II 52, 169–191.

Wiles, G.C., Barclay, D.J., Calkin, P.E., 1999. Tree-ring-dated 'Little Ice Age' histories of maritime glaciers from western Prince William Sound, Alaska. Holocene 9, 163–173.

Wilks, D.S., 2011. Statistical Methods in the Atmospheric Sciences. Elsevier, Oxford.

Wu, L., Li, C., 2007. Warming of the North Pacific Ocean: local Air–Sea coupling and remote climatic impacts. J. Clim. 20, 2581–2601. http://dx.doi.org/10.1175/JCLI4117.1.

Xie, P., Arkin, P.A., 1997. Global precipitation: a 17-year monthly analysis based on gauge observations, satellite estimates, and numerical model outputs. Bull. Am. Meteorol. Soc. 78, 2539–2558.

Xiong, Q., Royer, T.C., 1984. Coastal temperature and salinity in the northern Gulf of Alaska. J. Geophys. Res. 89, 8061–8066.